Fabrication of an Injectable Star-polylactide/Thiolated Hyaluronate Hydrogel as a Double Drug-Delivery System for Cancer Treatment

Yifan Zhang, Min Fang, Zhiyi Tan, Yu-ang Zhang, Chun-yu Huang,* Lu Lu, Jinhuan Tian, Lihua Li,* and Changren Zhou

Read Online

ACCESS | Metrics & More | Article Recommendations | Supporting Information

ABSTRACT: Unsatisfactory solid-tumor penetration or rapid metabolism of nanomaterials limits their therapeutic efficacy. Here, we designed an injectable thiolated hyaluronate (HA-SH) hydrogel as a stable drug-releasing platform for in situ tumor treatment. Biodegradable star-shaped polylactide (S-PLLA) was first synthesized and fabricated to porous microspheres to encapsulate hydrophobic curcumin (Cur@S-PLLA), which was then blended with hydrophilic doxorubicin (Dox) and the HA-SH precursor to form composite in situ formable hydrogels [Cur@S-PLLA/(Dox)HA-SH]. The results showed that adding the microspheres improved the performance of the hydrogel, such as decreasing the gelation time from 1080 s to 960 s and also the swelling ratio. The mechanical strength increased from 27 to 45 kPa. In addition, the double drug system guaranteed a sustained release of drugs, releasing Dox at the early stage, with the continuous later release of Cur after gel swelling or S-PLLA degradation to achieve long-lasting tumor suppression, which inhibits the survival of cancer cells. The inhibitory effects of the hydrogels on MCF-7 were studied. The cell activity in the double-loaded hydrogel was significantly lower than that of the control groups, and apparent dead cells appeared in 2 days and fewer living cells with time. Flow cytometry revealed that the Cur@S-PLLA/(Dox)HA-SH group had the highest apoptosis ratio of 86.60% at 12 h, and the drugs caused the cell cycle to be blocked in phase M to reduce cell division. In summary, the innovative release platform is expected to be used in long-lasting tumor suppression and provides more ideas for the design of drug carriers.
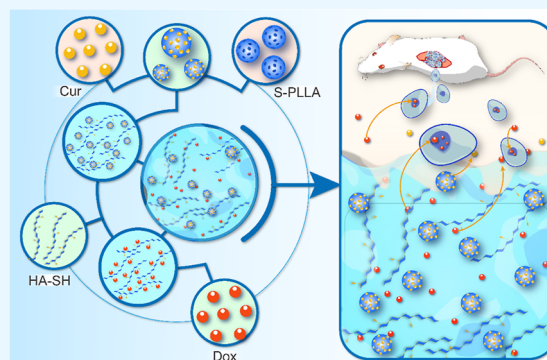
1. INTRODUCTION

Cancer is a malignant tumor originating from the epithelial tissue. The corresponding treatment is divided into surgical treatment, chemotherapy, radiotherapy, and targeted therapy according to the different properties, tissues, organs, disease stages, and reactions. However, some treatments have specific side effects, and even after the tumors are removed surgically, residual cancer cells are also at risk of recurrence.[1]

Doxorubicin (Dox) and curcumin (Cur) are two of the common antitumor medicines for chemotherapy. Dox is an antitumor antibiotic that inhibits the synthesis of RNA and DNA.[2] It is suitable for a wide variety of cancers, such as acute leukemia, breast cancer, malignant lymphoma, and so on.[3] However, its efficacy is limited by dose-dependent cardiotoxicity, which affects the hematopoietic function of the bone marrow.[4] Cur is a natural polyphenol found in the rhizome of some plants, has the properties of antitumor, anti-inflammatory, and anti-oxidation,[5] and is pharmacologically safe even at high doses.[6] It is well accepted that Cur inhibits tumor cell proliferation by blocking the activity of its transcription factor NF-κB and has several different molecular targets in the MAPK and PI3K/PKB's signaling pathways to inhibit proliferation and induce apoptosis in vitro.[7,8] Although Cur has numerous

advantages, its therapeutic application is limited because of its poor aqueous solubility, low stability against alkaline pH conditions, extensive first-pass metabolism, and rapid systemic elimination.[9]

Direct drug administration will lead to varying drug concentrations in human bodies.[10] Too high a local drug concentration of hydrophilic Dox can easily cause toxicity, and too low a concentration of hydrophobic Cur will decrease the treatment efficiency. Therefore, a carefully designed carrier may significantly facilitate Dox and Cur delivery, control their release ratio, and broaden the range of possible pharmaceutical applications.

Various materials, such as hydrogel and nano-/microparticles have been studied extensively as drug carriers for anti-tumor treatment. Herein, a multimodal therapeutic nanoplatform fabricated by coencapsulation of chlorin e6 and
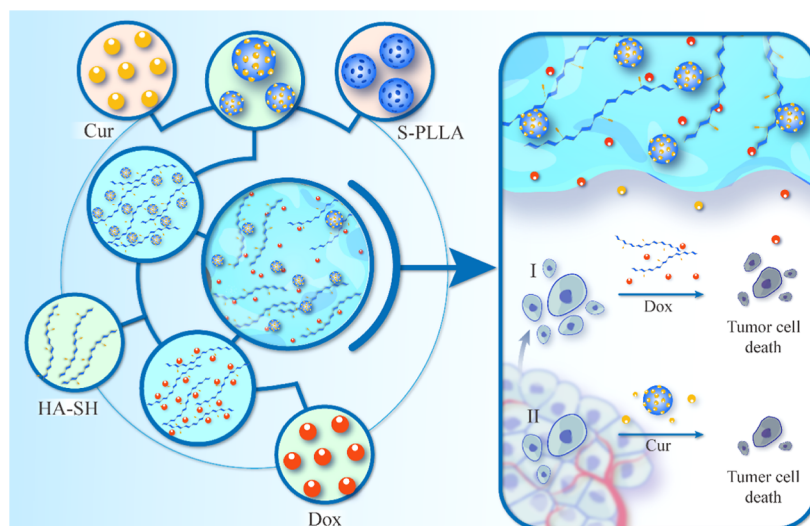
Figure 1. Schematic diagram of the preparation of double drug-loaded hydrogel and the sequential release of drugs in the tumor microenvironment.

tirapazamine (TPZ) with an amphiphilic polymeric conjugate of cisplatin and metronidazole is reported. This platform could kill the tumor periphery cells by the deeply penetrated oxygen-consuming sonodynamic therapy and unify the heterogeneously hypoxic content simultaneously, which then actuates the release and activation of the loaded TPZ.[11] To achieve the pH-responsive release of metformin (Met) in the tumor acidic microenvironment, oxidized hyaluronic acid (OHA)-Met was prepared by covalently grafting Met onto OHA through imine bonds, and then carboxymethyl chitosan (CMCS)/OHA-Met drug-loaded hydrogels were prepared. The CMCS/OHA-Met20 hydrogel could effectively kill MCF-7 cells while reducing the cytotoxicity of free Met toward L929 cells.[12] These biocompatible materials are used to achieve the purpose of both targeted therapy and chemical therapy, which can significantly improve the efficiency and utilization of drugs and reduce the hurt of cancer to patients.[13] Hydrogels are three-dimensional meshed colloidal materials with many water molecules.[14] Many natural polysaccharides such as chitosan, hyaluronate, and alginate-derived hydrogels, especially in situ formable hydrogels, have been fabricated and their application verified.[15−18] Because of their strong hygroscopicity, plasticity, and immunoregulation, they can be used as a multifunctional platform for drug release.[19−22]

Thiolation-modified polymers provide much higher adhesion properties than other polymers. The enhanced adhesion can be explained by the covalent bonds formed between the polymer and the mucus layer and the covalent bonds formed between the mucus layers, which are more potent than the noncovalent bonds.[23] This results in a stronger adhesion between the material and the body fluid, which is more conducive to the apposition of the cells to the material. At the same time, the interaction of the thiolated polymer with the cell membrane leads to a structural reorganization of the tightly attached proteins, thus enhancing the uptake of hydrophilic drugs by the cells.[24] Some investigators have used thiolated hyaluronate (HA-SH) scaffolds wrapped with polymeric nanoparticles to form a hybrid drug-delivery system to prevent peritoneal adhesions, and HA-SH is effective in preventing adhesions. In addition, animal studies have demonstrated the biocompatibility of HA-SH.[25]

In order to inhibit cancer more effectively and at the same time facilitate its use, we propose to design a hydrogel that can be molded in situ to act as a carrier from which the drug can be released. Initially, one drug could be released rapidly to inhibit cancer cells, and then another drug would be released slowly to destroy the remaining cancerous tissue. The ideal outcome of this material would be that the drug's slow release would inhibit cancer's recurrence after suppressing cancer. The study will be explored in vitro.

In this study, biocompatible HA-SH was synthesized to prepare an injectable hydrogel as a platform to release the hydrophilic Dox for further in situ treatment of solid tumors. Most of the drug was released fast to kill and restrain cancer cells at the early stage of the treatment. Then, another hydrophobic drug must be added to achieve a long-lasting anti-tumor effect.

Figure 1 shows the fabrication scheme of the injectable double drug-release system. Cur is encapsulated in the porous star-shaped poly L-lactide (S-PLLA) microspheres and dispersed in the Dox/HA-SH precursors to strengthen the hydrogel. The composite hydrogels are expected to be used for local immobilization and sustained release of drugs, which release Dox at the beginning and then continue to release Cur after gel swelling or PLLA degradation to inhibit the proliferation of tumor cells.

2. EXPERIMENTAL SECTION

2.1. Materials. L-Lactide was purchased from Macklin. Tin(II) 2-ethylhexanoate [Sn(Oct)$_2$, 95%], and pentaerythritol (≥99%) were purchased from Sigma-Aldrich; hyaluronic acid was purchased from Huaxi Furuida; L-cysteine hydrochloride monohydrate (L-cys, Sigma-Aldrich), 1-ethyl-3-(3-dimethylaminopropyl) carbodiimide hydrochloride (EDAC), N-hydroxy succinimide (NHS), and β-glycerophosphate disodium salt (β-GP) were of analytical grade and purchased from Qi Yun Biotechnology; Dox hydrochloride was purchased from Meryer; Cur was obtained from Shuoheng Biotechnology.

2.2. Synthesis and Characterization of S-PLLA. S-PLLA was prepared via ring-opening polymerization of L-lactide. Typical procedures were employed for preparing the 4-arm PLLA.[26] Pentaerythritol (3.93 mg, 2.9×10^{-2} mmol), Sn(Oct)$_2$ (17.6 mg, 4.34×10^{-2} mmol), and L-lactide(5 g, 34.7

mmol) were added to a dry glass ampule equipped with a magnetic stirrer. After purging with dry nitrogen six times, the ampule was sealed under vacuum and kept in an oil bath of 140 °C for 24 h. The products were dissolved in chloroform and then transferred into excess methanol for precipitation, and the process was repeated three times. After drying in a vacuum oven overnight at room temperature, 4-arm S-PLLA was obtained.

The S-PLLA was characterized by ^{1}H nuclear magnetic resonance (^{1}H NMR, AVANCE III 500NMR, Bruker) spectroscopy. Briefly, S-PLLA was dissolved in a deuterated chloroform solution and characterized by ^{1}H NMR. S-PLLA powder was mixed with KBr uniformly and pressed into a flaky shape, which was then characterized by Fourier transform infrared spectroscopy (FT-IR, Equinox 55, Bruker) with total reflection scanning. The molecular weight and distribution of S-PLLA were determined by gel permeation chromatography (GPC, Water1515, Water), in which tetrahydrofuran was the mobile phase with a flow rate of 1.0 mL/min, and the test temperature was 40 °C.[27] The narrow distribution of polystyrene was used as the working curve for the standard GPC.

2.3. Fabrication of Cur-Loaded S-PLLA Microspheres.
The 4-arm S-PLLA was dissolved in tetrahydrofuran at 55 °C with 2% w/v. Under rigorous mechanical stirring (1000 r/min), glycerol (55 °C) with three times the volume of S-PLLA solution was gradually added into the polymer solution. After stirring for 8 min, the mixture was quickly poured into liquid nitrogen. After 15 min, the water−ice mixture was added for solvent exchange for 24 h. The S-PLLA microspheres were sieved and washed with distilled water six times to remove residual glycerol on the sphere surface. The spheres were then lyophilized for 3 days.

The morphology of the freeze-dried S-PLLA microspheres was observed with scanning electron microscopy (SEM, PHILIPS XL-30ESEM).

The content of Cur in Cur ethanol solution and the encapsulation and loading rate of Cur in Cur-loaded S-PLLA (Cur@S-PLLA) were determined by using ethanol as the releasing medium using a spectrophotometer detector (Shimadzu, Japan). 0.1 g of 30, 60, and 90 mg/L Cur@S-PLLA microspheres were put into 15 mL centrifuge tubes, and 10 mL of ethanol was added. After the microspheres turned white and the drug was released, the release medium was taken to determine the ultraviolet adsorption value (A) at 425 nm. The A value of Cur@S-PLLA microspheres was substituted into the standard equation to calculate the entrapment efficiency (EE) and loading content (LC).

The EE was calculated using the formula

$$EE = \frac{\text{actual drug content}}{\text{total drugs in the system}} \times 100\%$$

The LC was calculated using the formula

$$LC = \frac{\text{actual drug content}}{\text{total mass of drug} - \text{carrying materials}} \times 100\%$$

2.4. Synthesis of Sulfhydrylated Hyaluronate (HA-SH).
2.0 g of HA was dissolved in 500 mL of deionized water, and EDAC and NHS were added at a final concentration of 50 mmol/L. 1 mol/L HCl was slowly added to adjust the pH of the reaction solution to 5−6, with continuous stirring for 30 min. Afterward, 4.0 g of L-cysteine hydrochloride monohydrate

(L-cys) was added to the reaction solution, and 1 mol/L NaOH was slowly added to adjust the pH to 5. After reacting for 5 h in the dark at room temperature under stirring, the product was dialyzed (MWCO 14 kDa) against HCl solution (pH = 5, containing 1 wt % NaCl) and finally freeze-dried.[28] The composition of HA-SH was characterized by ^{1}H NMR and FT-IR with an attenuated total reflectance accessory. The 1H NMR and Ellman's method determined the degree of substitution of HA-SH.

2.5. Preparation of Drug-Loaded Hydrogels.
2.5.1. Preparation of Cur@S-PLLA/HA-SH Hydrogel. HA-SH was dissolved in deionized water to obtain a concentration of 4% (w/v). β-GP was added to a final concentration of 8% (w/v) and stirred to achieve a homogenous solution with the pH of about 7. Afterward, Cur@S-PLLA microspheres of different concentrations (30, 60, and 90 mg/L) were dispersed into the solution with different concentrations (30, 60, and 90 mg/L) under magnetic stirring. The hydrogel precursors were placed in a 37 °C environment for gelation, and the hydrogels were denoted as (Dox)HA-SH.

Loaded with both Cur@S-PLLA and Dox, the hydrogels were denoted as Cur@S-PLLA/(Dox)HA-SH.

2.5.2. Rheological Analysis of Hydrogels. The hydrogel precursor with different drug contents was dropped on the rotary rheometer's sample table. A frequency scan (37 °C, 1% strain, and frequency of 1 Hz) was performed (DHR, Waters).

2.5.3. Gelation Time. The gelation time was determined by the vial inversion method. 1 mL of the hydrogel precursor was put in a glass bottle in a constant temperature water bath at 37 °C. The liquid fluidity was observed every 1 min until the sample in the bottle was no longer flowing, and the time was recorded ($n = 3$).

2.5.4. Swelling Ratio. The hydrogel samples were lyophilized and weighed as W_d. Then, they were put into 50 mL centrifuge tubes, and deionized water was added. The centrifuge tubes were put into a thermostatic shaker. At the time points of 10, 20, 30, 40, 50, 60, 120, 180, and 240 min, they were taken out and weighed after wiping the surface moisture and recorded as W_s. The swelling ratio (Q) was calculated by the following equation ($n = 3$):

$$Q = W_s/W_d$$

2.5.5. Compression Test. The hydrogel samples (Ø15 mm × 6.5 mm) were subjected to a compression test (1 mm/min, 60% deformation, $n = 5$) and a cyclic compression test ($\nu = 0.05$ Hz, 20 cycles, $n = 5$) with a JINJIAN testing machine.

2.6. In Vitro Drug Release.
(Dox)HA-SH hydrogels were placed in 30 mL of phosphate buffer solution (PBS, pH = 7.4/5.5). The experiment was performed in triplicate at 37 °C with shaking at 100 rad/min. All samples were withdrawn at preset time intervals and replaced with fresh PBS each time. A UV spectrophotometer measured the absorbance of three parallel samples at 485 nm. The samples were analyzed by a UV spectrophotometer (UV-2550, Shimadzu).

Dox/HA-SH hydrogels in PBS at pH 7.4 and 5.5 were used as in vitro release environments. The standard curves are as follows

$$A = 0.01990c - 6.6667 \times 10^{-5},$$
$$R^2 = 0.99993 \ (\text{pH} = 7.4)$$
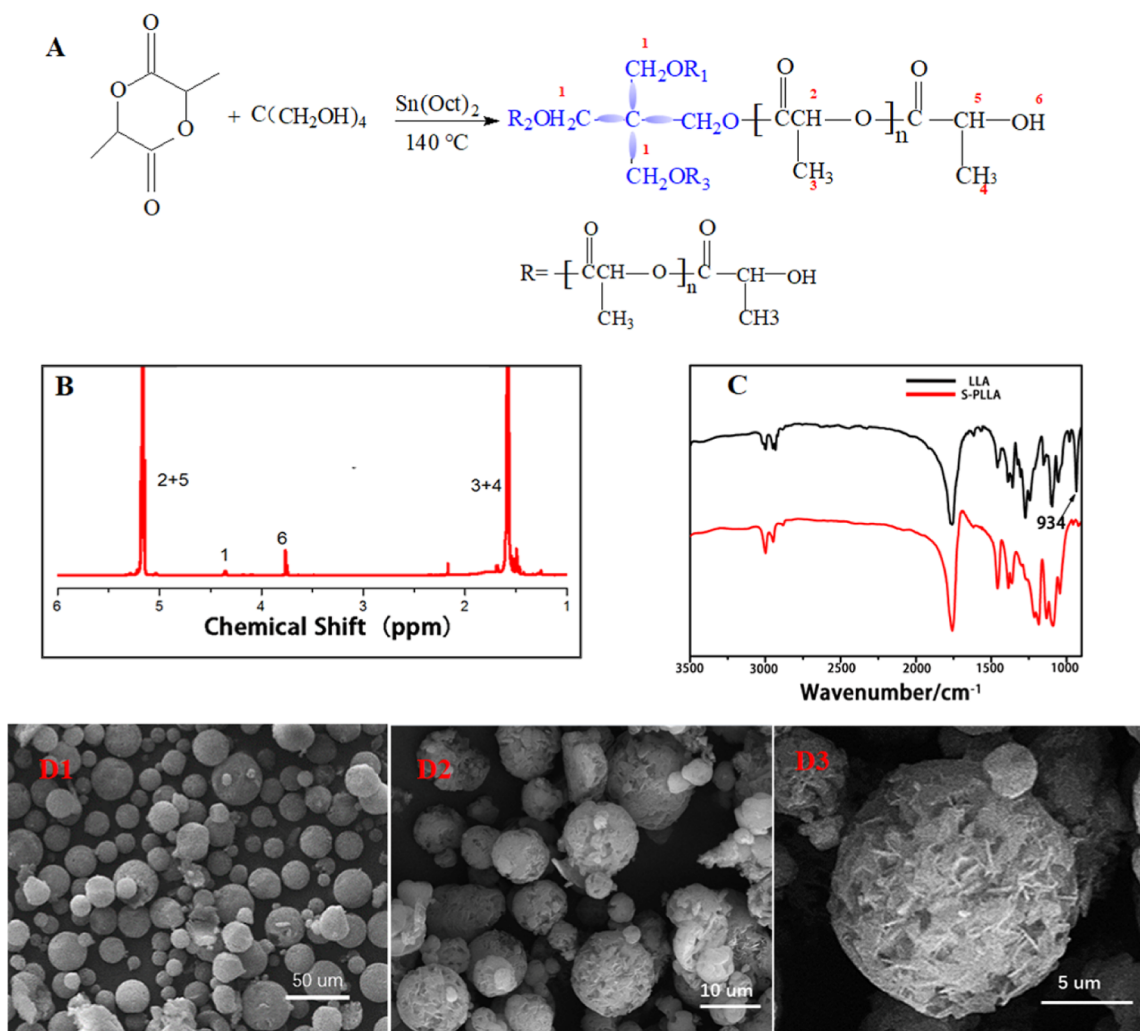
Figure 2. Synthesis and characterization of S-PLLA. (A) Reaction diagram. (B) ^{1}H NMR spectrum. (C) FT-IR spectra of L-lactide and S-PLLA. (D) SEM images of the S-PLLA microspheres with different magnifications.

$$A = 0.02243c - 0.0016, \quad R^2 = 0.9999 \ (pH = 5.5)$$

In vitro release of Cur was investigated in PBS containing 2% (v/v) Tween-80. Briefly, Cur@S-PLLA/HA-SH hydrogels (30 mg/L, 60 mg/L, and 90 mg/L) were placed in 50 mL centrifuge tubes, and the remaining was dialyzed in a dialysis bag (8000 Da) in 30 mL of release medium (pH = 7.4/5.5). The experiment was performed in triplicate at 37 °C with shaking at 100 rpm. All samples were withdrawn at preset time intervals and replaced with fresh PBS containing 2% Tween-80 each time. A UV spectrophotometer measured the absorbance of three parallel samples at 425 nm. The samples were analyzed by a UV spectrophotometer (UV-2550, Shimadzu).

Cur/S-PLLA/HA-SH hydrogels were released in PBS containing 2% Tween-80 at pH 7.4 and 5.5 as the in vitro release environment, with the following standard curves

$$A = 0.05007c - 5.33 \times 10^{-4},$$
$$R^2 = 0.99995 \ (pH = 7.4)$$

$$A = 0.04987c - 8 \times 10^{-4},$$
$$R^2 = 0.99992 \ (pH = 5.5)$$

2.7. Drug-Loaded Gel-Treated MCF-7 Cells. MCF-7 cells (a human breast cancer cell line) were cultured in 90% (v/v) Dulbecco' s modified Eagle's medium (DMEM) with 10% (v/v) fetal bovine serum and 1% penicillin/streptomycin solution in a humidified atmosphere at 37 °C containing 5% CO_2. The gels were placed in 24-well culture plates, and each plate was seeded with 1 mL of the MCF-7 cell suspension (1×10^4 cell/mL) and incubated for 24, 48, 72, and 96 h or some certain time.

2.7.1. CCK-8 Assay. The cell viability was evaluated using the CCK-8 assay. Briefly, the old culture medium was discarded and washed after culture for a predetermined time. 300 μL of the new culture medium and 30 μL of the CCK-8 solution were added into the well and then incubated for 2 h at 37 °C. The solution was then transferred to a new 96-well plate for the test, and the CCK-8 solution without cells was used as the blank control. The solution was measured by a microplate absorbance reader (Epoch, BIOTEK) at 450 nm. The percentage of viability was calculated by the following equation (n = 9). No material was added to the control group; the blank group was HA-SH without drugs.

2.7.2. Live/Dead Assay. The viability of MCF-7 cells was also evaluated by a live/dead cell staining kit [acridine orange/ethidium bromide (AO/EB) assay kit, solarbio]. After
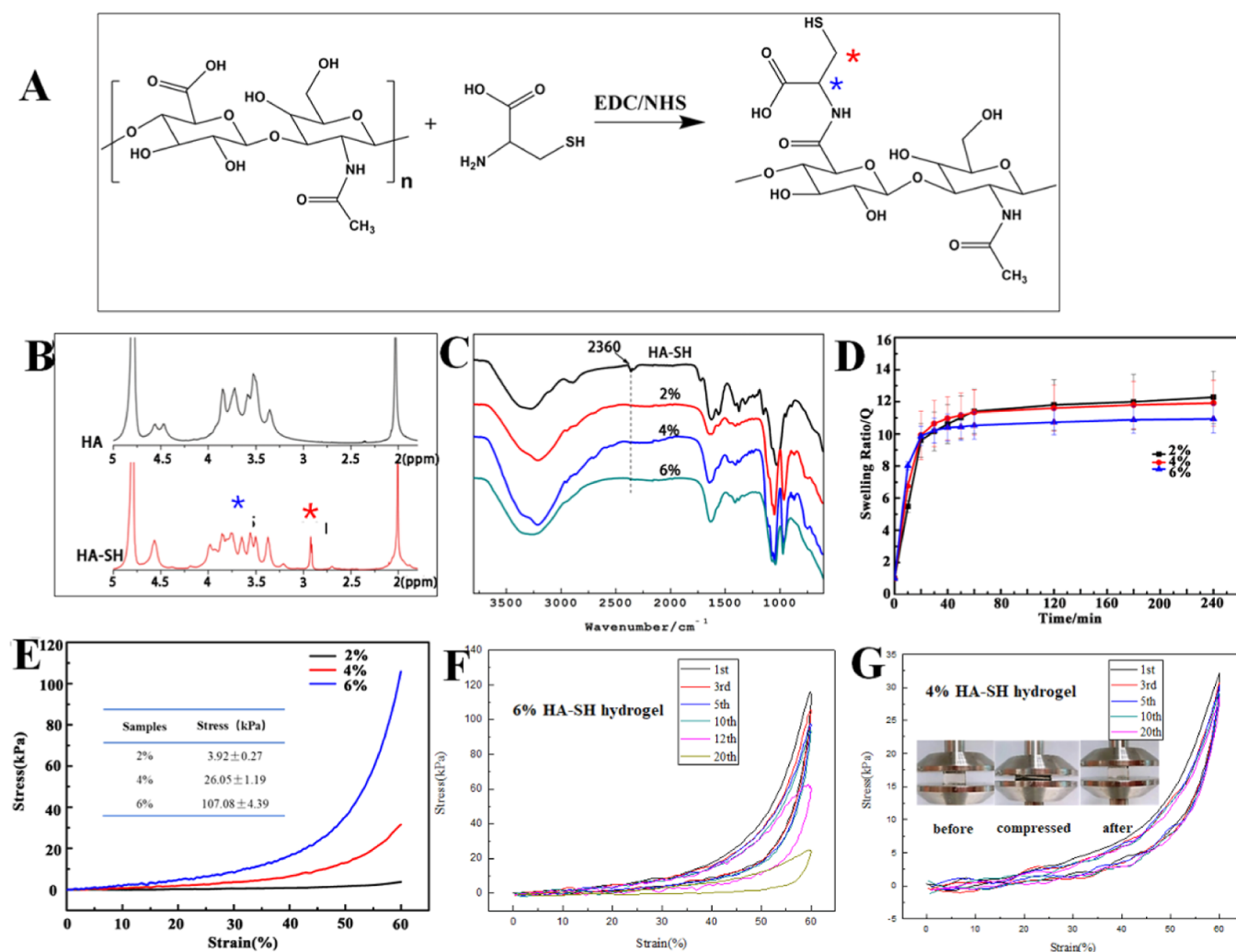
Figure 3. Characterization of HA-SH and the hydrogels with different concentrations. (A) Reaction diagram of HA and cysteine. (B) ^{1}H NMR spectra of HA and HA-SH. (C) FT-IR spectra of HA-SH and the hydrogels. (D) Equilibrium swelling ratio of the hydrogels in PBS at 37 °C. (E–G) Compressive and cyclic compressive stress–strain curves of the hydrogels. The inserted pictures show the hydrogels before compression, under compression, and after compression.

treatment for a preset time, the cells were washed with PBS three times. Then, the cells were incubated in AO/EB solution for 10 min at room temperature, washed with PBS, and observed immediately with a fluorescence microscope (Zeiss Axio Vert.A1). The control group is the no material added group, blank group for HA-SH hydrogel group.

2.7.3. Flow Cytometry. After 12 h of cell culture, the samples were washed three times with PBS, and the cells were collected by centrifugation. The cell pellets were resuspended in 0.5 mL of annexin buffer and stained with propidium iodide (PI) and annexin V-FITC containing binding buffer for 15 min and finally detected by flow cytometry (FACS Canto, BD Biosciences) for the apoptosis test.

After 48 h of cell culture, the samples were washed three times with PBS, and the cells were collected by centrifugation. The cell pellets were resuspended in 0.5 mL of 70% alcohol and placed in the refrigerator at 4 °C for 12 h. The suspension was stained with PI binding buffer for 15 min and finally detected by flow cytometry for the cell cycle test. The control group is the no material added group.

2.7.4. MCF-7 Cells for Drug Uptake. The Cur@S-PLLA/ (Dox)HA-SH gel was plated on a confocal dish, and MCF-7

cells (1×10^6 cells/well) were seeded and cultured in DMEM for 2, 6, 10, and 24 h. Then, the medium was discarded, and the samples were washed three times with PBS, followed by fixing with 4% paraformaldehyde for 15 min. The samples were washed with PBS and permeabilized with 0.1% Triton for 5 min. Finally, the samples were stained with 4′,6-diamidino-2phenylindole (DAPI), and the process of capturing Dox and Cur into cells was captured by confocal laser scanning microscopy (CLSM, LSM880, ZEISS). Control group is the HA-SH hydrogel group.

3. RESULTS AND DISCUSSION

3.1. Synthesis and Characterization of S-PLLA. L-Lactide and pentaerythritol were used to synthesize S-PLLA; the reaction process is shown in Figure 2A. The chemical composition was verified with ^{1}H NMR and FT-IR. Figure 2B shows that the hydrogen absorption peaks of methyl and methylene in the PLLA molecular structure are located at $\delta = 1.6$ ppm and $\delta = 5.1$ ppm, and the hydrogen absorption peaks of methylene appear at $\delta = 3.7$ ppm. The hydrogen absorption peak on the hydroxyl group appears at $\delta = 4.4$ ppm. As shown in Figure 2C, both lactide and S-PLLA have methyl stretching

Table 1. Encapsulation Efficiency and Drug-Loading Capacity of Cur@S-PLLA Microspheres[a]

sample	EE (%)	LC (%)
(30 mg/L) Cur@S-PLLA	10.3 ± 0.9	62.43 ± 5.87
(60 mg/L) Cur@S-PLLA	25.6 ± 1.1	81.16 ± 3.81
(90 mg/L) Cur@S-PLLA	35.5 ± 1.2	75.08 ± 2.60

[a]The ethanol standard curve of Cur: $A = 0.16683c - 0.01587$, R^2 = 0.9995.

vibration absorption peaks at wave number 2997 cm^{-1}, methylene stretching vibration peaks at 2936 and 2943 cm^{-1}, ester carbonyl vibration peaks at 1756 cm^{-1}, methyl bending vibration peaks at 1450 cm^{-1}, and methylene bending vibration peaks at 1354 cm^{-1}. In addition, the characteristic ring skeletal vibration peak of lactide at 934 cm^{-1} disappeared in the infrared spectrum of S-PLLA, which proved that the ring of lactide had been opened. The molecular weight distribution curve for S-PLLA is shown in Figure S1, with no multiple peaks. Peak 1 has a number average molecular weight of 21,328 and an average molecular weight of 34,348, with a PD value of 1.61 (Table S1).

S-PLLA porous microspheres were fabricated by emulsification and thermally induced phase separation. After a certain amount of glycerol was added to the stirred S-PLLA solution, an emulsion formed with multiple inner glycerol droplets inside one S-PLLA droplet. Upon quenching and freeze-drying, porous microspheres formed. In this study, the optimum condition for preparing S-PLLA microspheres was 4.0 wt % concentration, 800 r/min stirring rate, and 1:4 water−oil ratio. Figure 2D shows the morphology of the porous S-PLLA microspheres with increasing magnification. The diameter for the majority of the microspheres ranged from 10 to 20 μm.

It can be seen from Table 1 that due to its small mass compared with S-PLLA, Cur has a lower drug-loading capacity, while Cur@S-PLLA with 60 mg/L has the highest drug-loading capacity. The encapsulation efficiency of Cur@S-PLLA with 90 mg/L is the highest. Considering the total amount of drug encapsulation, the hydrogel with a Cur concentration of 90 mg/L will be used for the following double-load drug hydrogel experiments.

3.2. Characterization of HA-SH Hydrogels. The synthesis scheme of HA-SH is shown in Figure 3A. From the ^{1}H NMR spectra (Figure 3B), the absorption peak of the hydrogen atom at δ = 2.03 ppm did not change much before
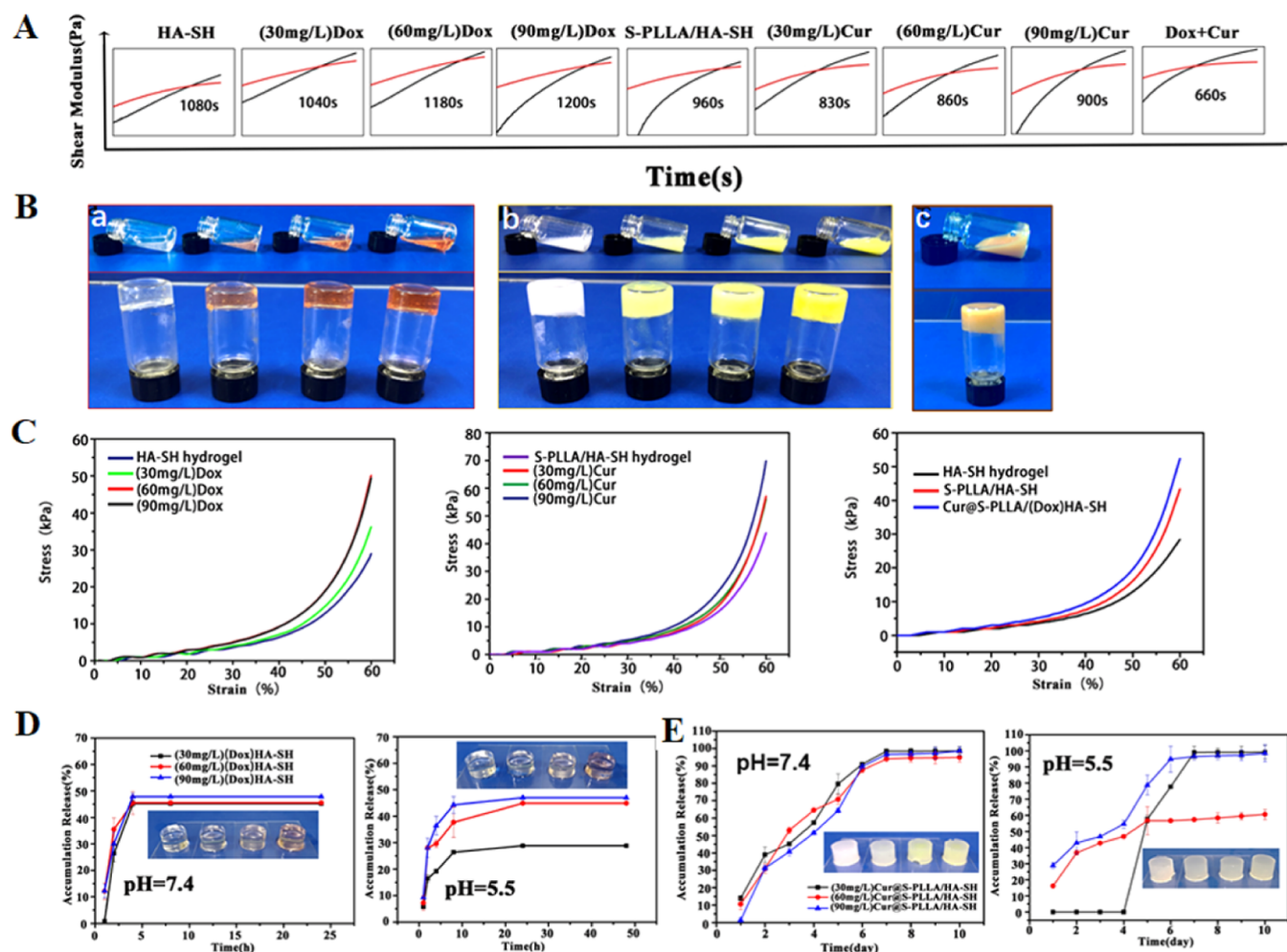
Figure 4. Characterization of the drug-loaded hydrogels with different concentrations of gel precursors. (A) Time-sweep of storage modulus and loss modulus during gelation. (B) Vial inverting measurement. (a) HA-SH and Dox/HA-SH hydrogels, (b) S-PLLA/HA-SH- and Cur-loaded hydrogels, and (c) Cur@S-PLLA/(Dox)HA-SH hydrogel. (C) Compressive stress−strain curves. (D,E) Drug in vitro release curves at pH 7.4 and 5.5. The pictures inserted are the images of the hydrogels after releasing drugs, and the first sample in each group is the blank control.
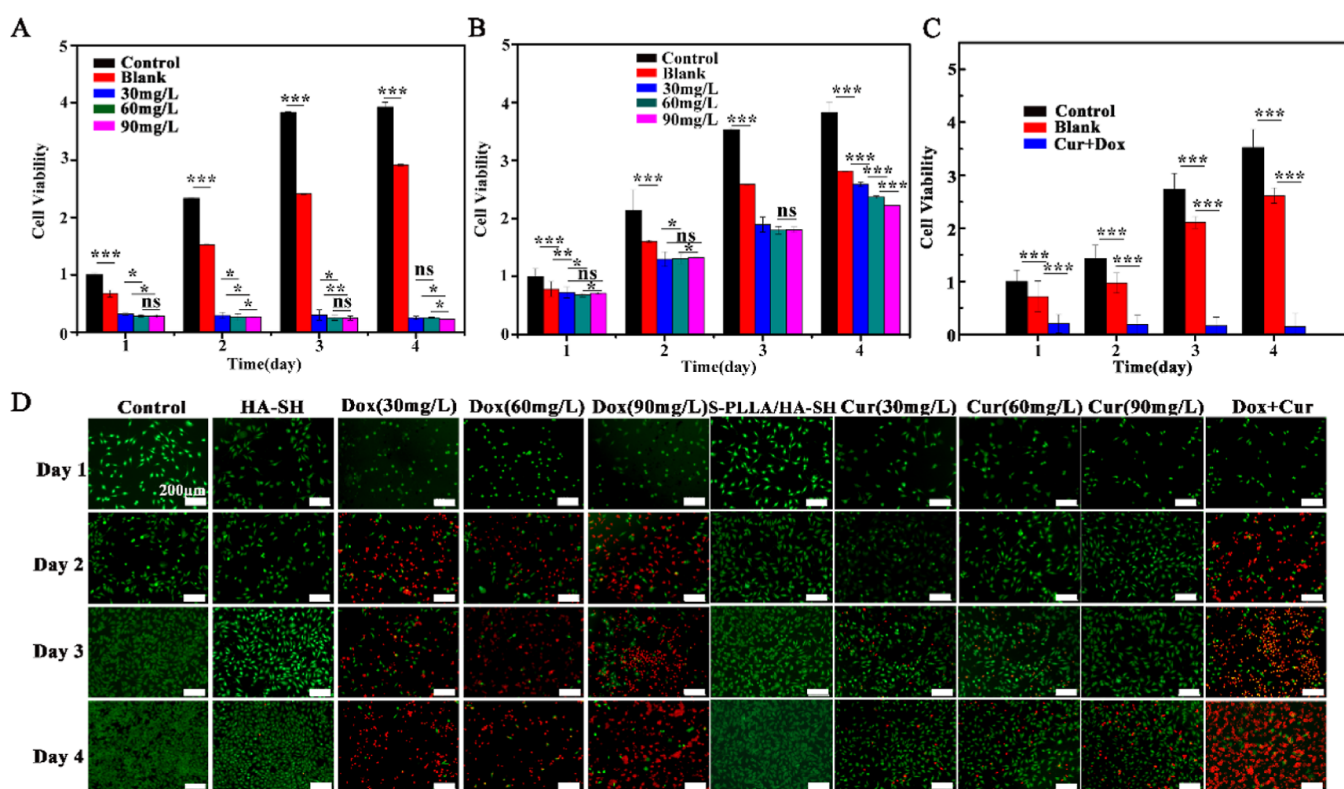
Figure 5. Cell culture results in different hydrogels. (A−C) Cell viability of MCF-7 by CCK-8 test in (Dox)HA-SH, Cur@S-PLLA/HA-SH, and Cur@S-PLLA/(Dox)HA-SH, respectively. (*$p < 0.05$, **$p < 0.01$, ***$p < 0.001$.) (D) AO/EB staining images of the drug-loaded hydrogels; green and red indicate living cells and dead cells, respectively; scale bar: 200 μm.

and after modification, representing the methyl absorption peak of −NHCOCH3 on the sugar ring of hyaluronic acid. Two new absorption peaks appear at $\delta = 2.91$ ppm and $\delta = 3.65$ ppm in HA-SH, attributed to the hydrogen absorption peaks of methylene and methenyl in-NHCH(COOH)CH2SH on the bonded cysteine molecule after modification. Figure 3C shows the FT-IR spectra of HA-SH hydrogels. There is an S−H stretching vibration peak at 2360 cm^{-1} in the HA-SH structure, but it disappears in the gel, which proves that the hydrogel is formed when the sulfhydryl group interacts on the side chain of HA. The new absorption peak at 968 cm^{-1} belongs to the characteristic absorption peak of the phosphate group of β-GP. Figure 3D shows that the 6% HA-SH hydrogel lyophilized sample has the lowest swelling ratio of 11.02 ± 0.67, originating from the network's higher density inducing lower water absorption. It also has the highest strength of 107 kPa at 60% deformation (Figure 3E). With increasing concentration, the hydrogel precursor solution gets more viscous and air-enwrapped, forming more heterogeneous gels. Therefore, the standard deviation values of the 6% samples are much larger than those of the other two. Cyclic compression test verified that the 6% samples are inclined to be deformed and fragmented; in contrast, the 4% samples are more elastic and can return near the original size after 20 times. Considering the processing and performance, a concentration of 4% will be used for the following experiment.

3.3. Characterization of Drug-Loaded Hydrogels. HA-SH solution is thermo-sensitive because of the −SH groups and H-bonding in the structure, which will be transformed to the hydrogel initiated by elevated temperature. The rheological study shows that the storage modulus (G') and loss modulus (G'') increase with time at 37 °C (Figure 4A). The cross point

is generally defined as the gelation point, and he corresponding time is the gelation time. For all hydrogels, the gelation time ranges from 660 to 1080 s (11−18 min), wherein the addition of Dox and S-PLLA microspheres increased or shortened the time, respectively. Vial inverting is not an accurate measurement for the gelation time, but the process from fluid to gel can be well recorded, as shown in Figure 4B. Compared to 27 kPa for the HA-SH hydrogel, the compressive strength was improved to about 50 and 70 kPa by adding Dox and S-PLLA microspheres, respectively (Figure 4C), and the value for the Cur@S-PLLA/(Dox)HA-SH hydrogel is about 55 kPa.

The release of Dox from hydrogels was relatively faster in both pH conditions (Figure 4D). There are no obvious differences between each sample at pH 7.4. It took about 4 h to arrive at the accumulative release ratio of 50%, which is also the maximum release ratio, with few drugs released with time. At pH 5.5, the release rate was a little lower. It took about 10−20 h to arrive at the maximum accumulative release ratio, 25% for (30 mg/L) (Dox)HA-SH and about 45% for (60 mg/L) (Dox)HA-SH and (90 mg/L) (Dox)HA-SH. Similarly, few drug releases even prolonged to 48 h. The main reason is the formation of H-bonding between the hydroxyl groups of the hydrophilic Dox and HA, which is beneficial for long-lasting in situ cancer treatment. Cur is hydrophobic and difficult to release at the beginning, so the drug is suitable for use with hydrophilic Dox for long-lasting treatment and prevents recurrence. We carried out the release test in vitro with the help of surfactants by a common approach.[29−31] Figure 4E shows that the drugs were released constantly in both conditions, except the Cur@S-PLLA/HA-SH samples at a pH of 5.5. It took about 6−8 days to arrive at the accumulative release ratio of nearly 100%. The photos of the hydrogels after
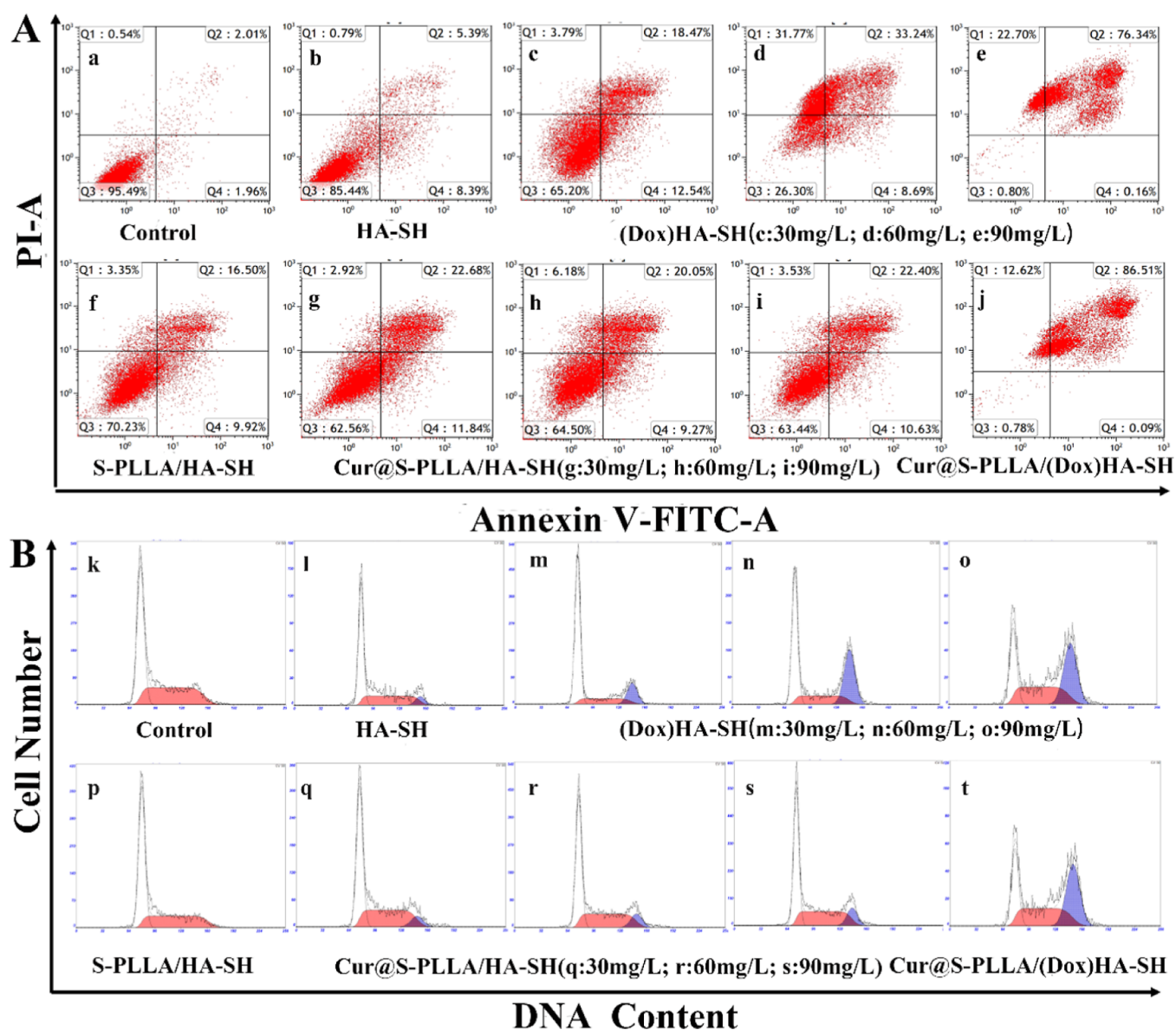
Figure 6. Flow cytometry results of the MCF-7 cells in drug-loading hydrogels. (A) Combination chart of the apoptotic test at 12 h. (B) Cell cycle test at 24 h.

Table 2. Cell Cycle Data for Drug-Loaded Hydrogels

	cell cycle		
sample	G0/G1 (%)	S (%)	G2/M (%)
blank	56.0	44.0	0
HA-SH	54.9	37.8	7.3
(30 mg/L) (Dox)HA-SH	64.5	18.6	17.0
(60 mg/L) (Dox)HA-SH	44.5	21.3	34.2
(90 mg/L) (Dox)HA-SH	25.4	36.5	38.1
S-PLLA/HA-SH	59.2	40.8	0
(30 mg/L) Cur@S-PLLA/HA-SH	50.3	42.5	7.2
(60 mg/L) Cur@S-PLLA/HA-SH	50.2	40.0	9.8
(90 mg/L) Cur@S-PLLA/HA-SH	48.1	40.2	11.7
Cur@S-PLLA/(Dox)HA-AH	22.4	33.5	44.1

Figure 7. Fluorescence images of MCF-7 cells in the Cur@S-PLLA/(Dox)HA-AH hydrogel at different time points (scale bar: 10 μm).

the release show that the appearance of the hydrogels did not change much in comparison with the blank control, indicating the relative stability during the short testing period.

3.4. Cell Culture Results on Drug-Loaded Hydrogels.

CCK-8 results of MCF-7 cell proliferation in the drug-loaded hydrogels were compared with the blank plate and corresponding blank hydrogels. The results showed that the HA-SH hydrogel showed good cellular compatibility. After the addition of Dox, the cell activity decreased significantly. With the extension of time, the cell activity did not change significantly (Figure 5A). There was no significant decrease in the cell activity of the compound hydrogel containing Cur, and the cell activity of the drug group increased with the extension of time (Figure 5B). The cell activity of Cur and Dox double-loading hydrogel was significantly lower than that of the HA-SH group, and the movement remained low for 4 consecutive days (Figure 5C). Figure 5D shows the images of live-dead staining of MCF-7 cells. Cells in the blank plate and the HA-SH hydrogel group had good morphology. The Dox-loaded group showed a higher number of dead cells on the second day, while the Cur@S-PLLA/HA-SH groups only showed apparent dead cells after day 3. The double drug-loaded hydrogels showed evident dead cells in 2 days, and there were fewer living cells and more dead cells with time. Cell culture results were obtained from a relatively isolated culture condition, and the data reflect an accumulative effect. Nevertheless, we can also conclude that the Dox-loaded system is a benefit for rapidly inhibiting cancer cells at the early stage of the treatment due to the fast release of Dox. Cur and S-PLLA are hydrophilic, so they cannot be released in a short time. The later slow release of Cur because of the gel swelling and PLLA degradation will benefit the long-lasting in situ treatment, especially for dense solid tumors.

The results of cell apoptosis detected by flow cytometry are shown in Figure 6A. Compared with the blank control group (a), the cell survival rate of the HA-SH hydrogel group (b) was lower, but there was no significant statistical difference. After adding Dox, the cell survival rate decreased significantly, and with the increase of Dox concentration, the cell survival rate gradually decreased (c−e). The apoptosis rate of 90 mg/L (Dox)HA-SH hydrogel was high at 76.50% at 12 h. The values for the Cur loaded S-PLLA/HA-SH hydrogels did not change much than that of the blank control (f−i). The Cur@S-PLLA/(Dox)HA-SH group had the highest apoptosis ratio of 86.60% (j).

The cell cycle of normal cells was mainly concentrated in the G0/G1 phase and S phase, as shown in Figure 6B and Table 2. With the addition of drugs, the G0/G1 phase cells were gradually decreased, while the cell numbers in the G2/M phase were steadily increased, with no apparent changes in the S phase cells. This phenomenon was shown in both Dox and Cur groups. The (Dox)HA-SH hydrogel was more pronounced (m−o). The addition of Cur and the variation of Cur content had little effect on the cell cycle (q−s). The most obvious impact was achieved by double-loading medicated hydrogels (t). According to the experimental results, the drug caused the cell cycle to be blocked in phase M. Phase M is the mitotic phase of cells, which can reduce cell division while repairing or inducing cell death to prevent the abnormal proliferation of cell mutations.[32] Dox and Cur selectively acted on the M phase of cancer cell MCF-7 and were involved in cell cycle regulation.

DAPI can dye the cell nucleus to emit blue fluorescence, and Cur and Dox can emit green and red fluorescence, respectively. MCF-7 cells were treated with the Cur@S-PLLA/(Dox)HA-SH gel after 0, 2, 6, 10, and 24 h, and the fluorescence images

by CLSM (Figure 7) showed the uptake process of Dox and Cur. It can be seen that the intensity of red fluorescence became more robust over time, indicating that more Dox entered the cells and inhibited the proliferation of MCF-7. In vitro release experiments demonstrated that Cur does not undergo release over a short period of time.

Based on the experimental results, the HA-SH hydrogel could gel and disperse Dox inside the gel quickly, and the S-PLLA microspheres successfully encapsulated Cur. The combination of the two successfully produced a dual drug-delivery system. It has the advantage that, as designed at the beginning, one of the drugs can be released rapidly in the initial phase with a significant inhibitory effect on the cancer cells. In the next phase, the other drug is released slowly in response to the degradation of the material and continues to inhibit the cancer cells. It is expected to achieve long-term tumor suppression and prevent tumor recurrence. Its limitation is that the release rate of curcumin is uncontrollable, and very minute amounts of the drug have little effect on cancer cells. In conclusion, this dual drug-loaded system could continue to be explored as a method of tumor suppression.

4. CONCLUSIONS

An injectable composite hydrogel as a double drug-release platform of Dox and Cur was fabricated. The results showed that hydrophilic Dox and hydrophobic Cur loaded micro-capsules (Cur@S-PLLA) could be well dispersed in the hydrogel, and the gel precursors can be injected in situ to form hydrogels within 15 min with good mechanical properties. The fast release of the Dox in the first stage and continuous release of the Cur were beneficial in inhibiting the growth of MCF-7 cells for a prolonged time. Therefore, the double drug-releasing platform is expected to be an innovative drug carrier for local injection and slow drug release and inhibits tumor growth.

■ ASSOCIATED CONTENT

ⓢ Supporting Information

The Supporting Information is available free of charge at https://pubs.acs.org/doi/10.1021/acsomega.3c00270.

> S-PLLA molecular weight distribution curve and S-PLLA molecular weight values (PDF)

■ AUTHOR INFORMATION

Corresponding Authors

Chun-yu Huang − *Department of Endoscopy, Sun Yat-Sen University Cancer Center, Guangzhou 510060, P. R. China;* Email: huangchy@sysucc.org.cn

Lihua Li − *Department of Materials Science and Engineering, Engineering Research Center of Artificial Organs and Materials, Jinan University, Guangzhou 511486, China;* Email: tlihuali@jnu.edu.cn

Authors

Yifan Zhang − *Department of Materials Science and Engineering, Engineering Research Center of Artificial Organs and Materials, Jinan University, Guangzhou 511486, China*

Min Fang − *Department of Materials Science and Engineering, Engineering Research Center of Artificial Organs and Materials, Jinan University, Guangzhou 511486, China*

Zhiyi Tan − *Guangzhou Customs District Technology Center, Guangzhou 510623 Guangdong, China*

Yu-ang Zhang − *Department of Materials Science and Engineering, Engineering Research Center of Artificial Organs and Materials, Jinan University, Guangzhou 511486, China*

Lu Lu − *Department of Materials Science and Engineering, Engineering Research Center of Artificial Organs and Materials, Jinan University, Guangzhou 511486, China;* orcid.org/0000-0002-6556-8022

Jinhuan Tian − *Department of Materials Science and Engineering, Engineering Research Center of Artificial Organs and Materials, Jinan University, Guangzhou 511486, China*

Changren Zhou − *Department of Materials Science and Engineering, Engineering Research Center of Artificial Organs and Materials, Jinan University, Guangzhou 511486, China;* orcid.org/0000-0003-2627-2293

Complete contact information is available at:
https://pubs.acs.org/10.1021/acsomega.3c00270

Notes

The authors declare no competing financial interest.

■ REFERENCES

(1) Liu, M.; Chen, D.; Mukerabigwi, J. F.; Chen, S.; Zhang, Y.; Lei, S.; Luo, S.; Wen, Z.; Cao, Y.; Huang, X.; et al. Intracellular delivery of 10-hydroxycamptothecin with targeted nanostructured lipid carriers against multidrug resistance. *J. Drug Targeting* **2016**, *24*, 433−440.

(2) Cao, W.; Chi, W.-H.; Wang, J.; Tang, J.-J.; Lu, Y.-J. TNF-α promotes Doxorubicin-induced cell apoptosis and anti-cancer effect through downregulation of p21 in p53-deficient tumor cells. *Biochem. Biophys. Res. Commun.* **2005**, *330*, 1034−1040.

(3) Epstein, A. L.; Taylor, C. R. Detection of necrotic malignant tissue and associated therapy, Google Patents. CA 1335720 C, 1999.

(4) Zhao, Y.; McLaughlin, D.; Robinson, E.; Harvey, A. P.; Hookham, M. B.; Shah, A. M.; McDermott, B. J.; Grieve, D. J. Nox2 NADPH Oxidase Promotes Pathologic Cardiac Remodeling Associated with Doxorubicin Chemotherapy. *Cancer Res.* **2010**, *70*, 9287−9297.

(5) Zhou, H.; S Beevers, C.; Huang, S.; Huang, S. The targets of curcumin. *Curr. Drug Targets* **2011**, *12*, 332−347.

(6) Shen, Y.; Tang, H.; Van Kirk, E.; Murdoch, W.; Radosz, M. Curcumin-Containing Polymers And Water-Soluble Curcumin Derivatives As Prodrugs Of Prodrug Carriers, US Patent. 20,120,003,177 A1, 2012.

(7) Safdari, Y.; Khalili, M.; Ebrahimzadeh, M. A.; Yazdani, Y.; Farajnia, S. J. Natural inhibitors of PI3K/AKT signaling in breast cancer: emphasis on newly-discovered molecular mechanisms of action. *Pharmacol. Res.* **2015**, *93*, 1−10.

(8) Chen, A.; Zheng, S. Curcumin inhibits connective tissue growth factor gene expression in activated hepatic stellate cells *in vitro* by blocking NF-κB and ERK signalling. *Br. J. Pharmacol.* **2008**, *153*, 557−567.

(9) Hasan, M.; Ben Messaoud, G.; Michaux, F.; Tamayol, A.; Kahn, C. J. F.; Belhaj, N.; Linder, M.; Arab-Tehrany, E. Chitosan-coated liposomes encapsulating curcumin: Study of lipid−polysaccharide interactions and nanovesicle behavior. *RSC Adv.* **2016**, *6*, 45290−45304.

(10) Laszczyk, M. N. Pentacyclic Triterpenes of the Lupane, Oleanane and Ursane Group as Tools in Cancer Therapy. *Planta Med.* **2009**, *75*, 1549−1560.

(11) Zhang, L.; Du, X.; Li, Q.; Qian, L.; Chen, J.; Liu, C.; Yu, Q.; Gan, Z. A Multimodal Therapeutic Nanoplatform Overcoming Tumor Hypoxia Heterogeneity for Improved Tumor Chemoradiotherapy. *Adv. Funct. Mater.* **2022**, *32*, 2204629.

(12) Zheng, Z.; Yang, X.; Zhang, Y.; Zu, W.; Wen, M.; Liu, T.; Zhou, C.; Li, L. An injectable and pH-responsive hyaluronic acid hydrogel as metformin carrier for prevention of breast cancer recurrence. *Carbohydr. Polym.* **2023**, *304*, 120493.

(13) Matsumoto, T.; Okazaki, M.; Nakahira, A.; Sasaki, J.; Egusa, H.; Sohmura, T. Modification of apatite materials for bone tissue engineering and drug delivery carriers. *Curr. Med. Chem.* **2007**, *14*, 2726−2733.

(14) Lu, W.; Li, H.; Huo, B.; Meng, Z.; Xue, M.; Qiu, L.; Ma, S.; Yan, Z.; Piao, C.; Ma, X. Full-color mechanical sensor based on elastic nanocomposite hydrogels encapsulated three-dimensional colloidal arrays. *Sens. Actuators B Chem.* **2016**, *234*, 527−533.

(15) Ye, B.; Zhang, S.; Li, R.; Li, L.; Lu, L.; Zhou, C. An in-situ formable and fibrils-reinforced polysaccharide composite hydrogel by self-crosslinking with dual healing ability. *Compos. Sci.* **2018**, *156*, 238−246.

(16) Li, R.; Liu, Q.; Wu, H.; Wang, K.; Li, L.; Zhou, C.; Ao, N. Preparation and characterization of in-situ formable liposome/ chitosan composite hydrogels. *Mater. Lett.* **2018**, *220*, 289−292.

(17) Lin, Z.; Li, R.; Liu, Y.; Zhao, Y.; Ao, N.; Wang, J.; Li, L.; Wu, G. Histatin1-modified thiolated chitosan hydrogels enhance wound healing by accelerating cell adhesion, migration and angiogenesis. *Carbohydr. Polym.* **2020**, *230*, 115710.

(18) Liu, Y.; Zhang, Y.; Zheng, Z.; Zhong, W.; Wang, H.; Lin, Z.; Li, L.; Wu, G. Incorporation of NGR1 promotes bone regeneration of injectable HA/nHAp hydrogels by anti-inflammation regulation via a MAPK/ERK signaling pathway. *Front. Bioeng. Biotechnol.* **2022**, *10*, 992961.

(19) Peppas, N.; Hilt, J.; Khademhosseini, A.; Langer, R. Hydrogels in Biology and Medicine: From Molecular Principles to Bionanotechnology. *Adv. Mater.* **2006**, *18*, 1345−1360.

(20) Augst, A. D.; Kong, H. J.; Mooney, D. J. Alginate hydrogels as biomaterials. *Macromol. Biosci.* **2006**, *6*, 623−633.

(21) Sun, K.; Yu, J.; Hu, J.; Chen, J.; Song, J.; Chen, Z.; Cai, Z.; Lu, Z.; Zhang, L.; Wang, Z. Salicylic acid-based hypoxia-responsive chemodynamic nanomedicines boost antitumor immunotherapy by modulating immunosuppressive tumor microenvironment. *Acta Biomater.* **2022**, *148*, 230−243.

(22) Badylak, S. F.; Freytes, D. O.; Gilbert, T. W. Extracellular matrix as a biological scaffold material: Structure and function. *Acta Biomater.* **2009**, *5*, 1−13.

(23) Bernkop-Schnürch, A.; Hornof, M.; Zoidl, T. Thiolated polymers—thiomers: synthesis and in vitro evaluation of chitosan−2-iminothiolane conjugates. *Int. J. Pharm.* **2003**, *260*, 229−237.

(24) Kast, C. E.; Bernkop-Schnürch, A. Thiolated polymers—thiomers: development and in vitro evaluation of chitosan−thioglycolic acid conjugates. *Biomaterials* **2001**, *22*, 2345−2352.

(25) Yeo, Y.; Ito, T.; Bellas, E.; Highley, C. B.; Marini, R.; Kohane, D. S. In situ cross-linkable hyaluronan hydrogels containing polymeric nanoparticles for preventing postsurgical adhesions. *Ann. Surg.* **2007**, *245*, 819−824.

(26) Zhang, Z.; Marson, R. L.; Ge, Z.; Glotzer, S. C.; Ma, P. X.; Sharon, C.; Peter, X. Simultaneous Nano- and Microscale Control of Nanofibrous Microspheres Self-Assembled from Star-Shaped Polymers. *Adv. Mater.* **2015**, *27*, 3947−3952.

(27) Chisholm, M. S.; Slark, A. T.; Sherrington, D.; O'brien, N. Polymer composition, US, Patent No. US10662418; 2004.

(28) Ding, J.; He, R.; Zhou, G.; Tang, C.; Yin, C. Multilayered mucoadhesive hydrogel films based on thiolated hyaluronic acid and polyvinylalcohol for insulin delivery. *Acta Biomater.* **2012**, *8*, 3643−3651.

(29) Zhang, Y.; Wischke, C.; Mittal, S.; Mitra, A.; Schwendeman, S. P. Design of controlled release PLGA microspheres for hydrophobic fenretinide. *Mol. Pharm.* **2016**, *13*, 2622−2630.

(30) Zhang, H. C.; Liu, J. M.; Chen, H. M.; Gao, C. C.; Lu, H. Y.; Zhou, H.; Li, Y.; Gao, S. L. Up-regulation of licochalcone A biosynthesis and secretion by Tween 80 in hairy root cultures of Glycyrrhiza uralensis Fisch. *Mol. Biotechnol.* **2011**, *47*, 50−56.

(31) Li, F.; Zhu, A.; Song, X.; Ji, L. Novel surfactant for preparation of poly(L-lactic acid) nanoparticles with controllable release profile and cytocompatibility for drug delivery. *Colloids Surf., B* **2014**, *115*, 377−383.

(32) Amara, A. A. F. The inevitability of balanced lives: Genes and, foods in action and, interactions. *IIOAB J.* **2013**, *4*, 1−27.